Single-layer graphene nanosheets with controlled grafting of polymer chains†

Ming Fang,[a] Kaigang Wang,[a] Hongbin Lu,*[a] Yuliang Yang[a] and Steven Nutt[b]

Received 14th September 2009, Accepted 19th November 2009
First published as an Advance Article on the web 21st January 2010
DOI: 10.1039/b919078c

Single-layer graphene nanosheets (SLGNs) are prepared by reduction of well-exfoliated graphite oxide aided by a surfactant (sodium dodecylbenzene sulfonate, SDBS). Grafting density and polystyrene (PS) chain lengths are controlled by modulating the concentrations of diazonium compound and monomer during the grafting reaction of the initiator and the succeeding atomic transfer radical polymerization (ATRP). Atomic force microscopy (AFM), X-ray diffraction (XRD), Raman spectra and transmission electron microscopy (TEM) are used to confirm the single-layer structure of graphene sheets, covalent bonding at the interface, and distribution uniformity of grafting PS chains at the SLGN surface. Thermogravimetric analysis (TGA) is performed to assess the control of grafting density and chain length. PS chains grafted on the SLGN surface exhibited remarkably confined relaxation behavior. An increase in the glass transition temperature (T_g) of up to 18 °C is observed for high grafting density, low molecular weight polymer-grafted graphene samples. The low grafting density, high molecular weight sample shows an increase in T_g of ~9 °C, which is attributed to superior heat conduction efficiency. The measured thermal conductivity for the PS composite film with 2.0 wt% SLGNs increase by a factor of 2.6 compared to that of the pure PS.

1. Introduction

Graphene nanosheets (GNs) have received attention in efforts to develop high-performance functional materials.[1,2] For example, potential new applications based on GNs have been demonstrated, including transistors, photovoltaic electrodes, resonators, and ultracapacitors.[3–9] Likewise, polymer nanocomposites based on GNs have shown remarkable improvements in thermal and electrical properties, even at low GN loadings.[10,11] Two classes of approach, *i.e.*, "bottom-up"[12,13] and "top-down",[14–17] have been employed to prepare GN materials. The former allows tuning of the fine structure of GNs, such as size, shape, and even type and location of defects. This approach has established a basis for bandgap control, supramolecular assembly and device applications of GNs. The advantage of the latter approach lies in the abundant source material (natural graphite) and the potential for large-scale production. Among various "top-down" approaches, an intriguing route involves preparation of GNs by reduction of graphite oxide (GO). GO has multiple oxygen-containing functionalities, such as hydroxyl and epoxide groups in the basal plane, and carboxyl groups at plane edges.[2] Consequently, GO is readily dispersed in water and polar solvents, such as DMF.[18–20] This characteristic facilitates preparation of different polymer nanocomposites by solution processing. However, reduction typically causes irreversible particle aggregation in solvents due to the prominent interlayer π–π conjugate interaction of GNs, particularly for large GNs.[21,22] The interlayer cohesive energy of GNs increases sharply with increasing surface area, which interferes with the dispersion of GNs in matrices and the interaction between GNs and polymers.[23] In this regard, molecular dynamic simulations have shown that the volume exclusion effect of grafting molecules contributed to weaken such interlayer interactions of GNs, facilitating their dispersal in solvents and polymers.[24,25] This implies that surface decoration of GNs is a crucial issue for the development of polymer nanocomposites.

In polymer nanocomposites, interfaces typically constitute much larger volume fractions than in conventional particle-filled composites.[26,27] This factor has a profound effect on the microstructure evolution and relaxation dynamics, which arises from variations in the total free energy of systems.[28,29] For example, a well-wetted particle surface in a polymer host can minimize the enthalpic interaction so that the distribution of particles and dynamic behavior are primarily driven by the system entropy.[30] For such particle–polymer systems, the relaxation behavior of polymer chains largely depends on characteristics of the interface. Typically, the relaxation rate of polymer chains (or interaction between particles and matrices) can be tuned by changing interface parameters, such as grafting density and grafting chain length of polymers on particles.[10,31] Thus, in order to optimize the performance of GN-based nanocomposites, an effective method to tailor the interface structure must be developed.

For this purpose, non-covalent[32–34] and covalent functionalization[2,35–41] approaches have been proposed. Early efforts with exfoliated GNs involved chemical reduction of GO in the presence of polyelectrolytes (*e.g.*, poly(sodium 4-styrene sulfonate)).[34] Polyelectrolyte-assisted preparation enables the resultant GNs to stably disperse in water or polar solvents, but this renders the GNs incompatible with non-polar solvents or polymers and thus presents difficulties for a wide range of

[a]*The Key Laboratory of Molecular Engineering of Polymers of Ministry of Education, Department of Macromolecular Science, Fudan University, Shanghai, 200433, China. E-mail: hongbinl@fudan.edu.cn; Fax: +86-21-55664589; Tel: + 86-21-55664589*
[b]*Department of Chemical Engineering and Materials Science, University of Southern California, Los Angeles, CA, 90089-0241, United States*
† Electronic supplementary information (ESI) available: Molecular sizes of grafted PS and free PS. See DOI: 10.1039/b919078c

potential applications. The use of surfactants is effective for preparing single-layer GNs, and can transfer GO-reduced GNs from aqueous phases to organic phases and thereby preserve stable dispersions.[8] In this approach, the solubility of surfactants in the two phases must be balanced.[8] An alternate approach, covalent decoration, has also been employed to improve the dispersion of GNs in polymers. Phenyl isocyanate has been shown to facilitate the dispersion of GNs in polystyrene by reacting with hydroxyl and carboxyl groups residing on GN surfaces after reduction.[11,37,38] Other aromatic molecules such as nitrophenyl and porphyrin have also been covalently bonded to the GN surface by employing diazonium addition and formation of amide bonds. This method prevents aggregation and affords an opportunity to tune the bandgap energy of GNs by introducing defects.[39,40] However, this approach to tailoring GN–polymer interfaces poses difficulties because of the small molecule size. To address this difficulty, poly(vinyl alcohol) (PVA) has been used to covalently functionalize multi-layer GNs (MLGNs) by the reaction between the residual carboxyl groups on GNs and the hydroxyl groups of PVA chains.[42] The resulting GNs demonstrated enhanced dispersion capacity in DMSO and hot water. However, this method generally requires polymers containing hydroxyl groups. In a previous work,[43] we have reported a method to functionalize MLGNs by combining diazonium addition with atomic transfer radical polymerization (ATRP). By decreasing the size of GNs to 20–40 nm, their interlayer cohesive energy was remarkably reduced so that no pronounced GN aggregation occurred during the grafting reaction of polymer even without the protection of surfactants. Smaller dimensions facilitate the dispersal of GNs in polymers but at the cost of compromising the thermal or electrical properties of GNs. To take full advantage of the exceptional properties of GNs, it is desired to achieve controllable interface decoration of large, single-layer GNs (SLGNs).[44]

In this work, we report the first effort to systematically tune the interface structure of SLGNs (average lateral size of ~1 nm) with covalently grafted polystyrene (PS) chains. Controlled diazonium addition was found to be effective for tuning the grafting density of PS on SLGNs. Living ATRP was utilized to tailor the chain length of grafting PS. We demonstrate the peculiar relaxation behavior of polymer chains grafted on SLGNs, as well as the substantial increase in thermal conductivity of polymer composite films.

2. Experimental

2.1. Preparation of single-layer graphite oxide sheets (GO)

Graphite powder (Qingdao BCSM Co. Ltd., China) was used to prepare exfoliated GO sheets following a well-established method.[44] $NaNO_3$, sulfuric acid and $KMnO_4$ were used to oxidize the graphite powder, after which individual GO sheets were stably dispersed in water. After exhaustive washing, the resulting GO sheets were dried at 65 °C in vacuum.

2.2. Synthesis of hydroxyl-bonded graphene sheets (HO-GNs) and control of grafting density

Varying the concentration of the diazonium compound during the grafting reaction was an effective method for controlling the bond density of the initiator and thus the grafting density of polymer chains. In our experiments, the diazonium compound was controlled by changing the concentration of both 2-(4-aminophenyl)ethanol and isoamyl nitrite in the system. A typical procedure was employed as follows. GO (60 mg) was dispersed in 150 mL de-ionized water containing 150 mg surfactant (sodium dodecylbenzene sulfonate, SDBS). After stirring and sonication for 30 min, hydrazine hydrate (50%, 0.3 mL) was slowly added to the suspension, refluxing at 100 °C for 14 h. Subsequently, 2-(4-aminophenyl)ethanol and isoamyl nitrite were added, and the mixture was stirred continuously at 80 °C overnight. After cooling to room temperature, the suspension was filtered using a Teflon filter and washed exhaustively with de-ionized water and N,N-dimethylformamide (DMF) until the filtrate was clear. The resulting black solid (HO-GNs) was dried under vacuum. Two grafting densities (low and high) of the initiator were bonded to the GN surface, and the concentration of diazonium compound for the high initiator density was four times that of the low initiator density.

2.3. Synthesis of initiator-bonded graphene sheets (Init-GNs)

All operations must be implemented in nitrogen atmosphere. In a typical process, dried HO-GNs (50 mg) were dispersed in THF (40 mL) containing 0.1 mL triethanolamine. The suspension was then cooled to 0 °C, and excess 2-bromopropionyl bromide (0.43 g, Alfa Aesar, 2 mmol) was added dropwise. Further stirring was conducted at 0 °C for 2 h and at room temperature for 24 h. The suspension was then filtered and washed repeatedly with de-ionized water and DMF to remove un-reacted organics. The black solid obtained was dried overnight at 40 °C under vacuum.

2.4 Synthesis of polystyrene-grafted graphene nanosheets (PS-GNs)

The chain length of grafting PS was varied in this stage by changing the monomer/initiator ratio. Three ratios (250 : 1, 500 : 1 and 1000 : 1) were used to prepare the grafting polymers with low, moderate and high molecular weights. For the high molecular weight sample (PS3-2-GNs, see Table 1), the synthesis process was as follows. Init-GNs (50 mg) were dispersed in 1,2-dichlorobenzene (DCB, 8 mL) containing styrene (St, Alfa Aesar, 10.4 g), methyl-2-bromopropionate (BMP, Alfa Aesar, 16.7 mg; 0.10 mmol) and CuBr (30 mg, 0.20 mmol). The suspension was degassed by three freeze-pump-thaw cycles, to which N,N,N′,N′,N′-pentamethyl-diethylenetriamine (PMDETA, Alfa Aesar, 0.0417 mL, 0.2 mmol) was added with a syringe. Subsequently, the suspension was immersed immediately in an oil bath at 110 °C and stirred continuously for 14 h. The mixture was cooled, diluted with additional THF, and vacuum-filtered using a Teflon filter. The filtrate was passed through a column chromatograph filled with neutral alumina to remove the copper complex and precipitated with methanol (200 mL). After filtration, the product was purified twice by dissolution-precipitation with methanol and dried at 40 °C for 17 h under vacuum. The gray solid obtained by filtration was washed with DMF (100 mL) three times and dried at 40 °C under vacuum.

Table 1 The reaction conditions and experimental results of different PS-grafted GNs

Sample	[M]/[I]/[CuBr]/[PMDETA][c]	Reaction time/h	Yield (%)	$M_{n,GPC}$[d]	M_w/M_n	Weight loss (wt%) at 600 °C[e]
PS-1-GNs[a]	1000 : 1 : 2 : 2	14	82	81 600	1.56	55.4
PS1-2-GNs[b]	250 : 1 : 2 : 2	14	85	21 300	1.60	49.6
PS2-2-GNs[b]	500 : 1 : 2 : 2	14	71	35 600	1.90	61.7
PS3-2-GNs[b]	1000 : 1 : 2 : 2	14	79	78 900	1.65	85.5

[a] PS-1-GNs is a low grafting density sample. [b] PS1-, PS2- and PS3-2-GNs are three high grafting density samples. [c] The molar ratio of components. [d] Determined by GPC measurements at room temperature in which THF was used as an eluent and PS standard for the calibration. [e] Determined from the TGA curves with the measuring condition: 20 °C min^{-1} in nitrogen atmosphere.

2.5. Preparation of PS films containing graphene

The PS polymer matrix had a weight average molecular weight (M_w) of 350 000 and a polydispersity of 2.5 (Aldrich). PS-1-GNs and PS1-2-GNs were used to prepare the PS-GN nanocomposite films 0.35–0.5 mm thick. In a typical preparation procedure, different mass fractions of PS1-2-GNs were first dispersed in toluene by bath sonication at room temperature. The solutions obtained were then mixed with another toluene solution with 15 wt% PS by sonicating for 30 min at room temperature to achieve homogeneous suspensions. Finally, these suspensions were slowly dropped into clean glass dishes and dried in vacuum at 50 °C. The resulting films were peeled from the substrate prior to further thermal conductivity characterization.

2.6. Characterization methods

The molecular characteristics of grafting polystyrene (PS) were determined by gel permeation chromatography (GPC, Waters Breeze) by measuring the free polystyrene chains. Tetrahydrofuran (THF) was used as an eluent, and the PS standard was used for calibration. Atomic force microscopy (AFM, Multimode Nano 4) was used in tapping mode to characterize the morphology of GO, Init-GNs and PS-GNs. The set-point amplitude ratio was fixed at 0.9 to minimize tip-induced sample deformation. The samples for AFM observations were prepared by spin-coating dilute suspensions (GO in water and Init-GNs, PS-GNs in DMF) on freshly cleaved mica surfaces. Transmission electron microscopy (TEM, JEOL-1230) was used to observe the PS-GNs. To prepare samples suitable for TEM observation, different solvents were employed in an effort to control the morphology of PS on GNs and to permit simultaneous observation of GNs and PS. DMF was an effective solvent because the partially collapsed PS that formed after drying did not cover the entire surface of GNs. This was particularly important for observation of the low-density PS-grafted GN sample, such as PS-1-GNs. The interlayer spacings of GO and GN derivatives (dried powder samples) were measured using an X-ray diffractometer (Rigaku D/max-γB) with Cu-Kα radiation (= 1.54 Å) at a scanning rate 0.02° s^{-1} and an angle range from 5 to 60°. Raman spectra of GO and GN derivatives (dried powder samples) were obtained using a multi-channel confocal microspectrometer with a laser wavelength of 631 nm (Dilor LABRAM-1B). Thermogravimetric measurements were performed (Netzsch TG 209) from room temperature to 600 or 800 °C at 20 °C min^{-1} in nitrogen. The glass transition temperatures (T_g) of PS and PS-GNs samples were determined from differential scanning calorimetry (DSC, TA Q100) curves (heating rate: 10 °C min^{-1}). The thermal history of the samples was eliminated by heating them to 180 °C at 20 °C min^{-1} and holding for 5 min. All samples for DSC tests were prepared by a precipitating separation method from GO or GN suspensions, followed by exhaustively washing and vacuum drying. For thermal conductivity measurements, the densities of samples (ρ) were first determined (Mettler Toledo density Kit AL 204) using ethanol as an assistant liquid. The specific heat capacities (C_p) of the samples were measured by modulated DSC (TA Instruments Q100). Thermal diffusivity (α) was obtained using a light flash system (Netzsch LFA 447 Nanoflash, with xenon flash lamp, 304 V, and long pulse) at 35 °C. The thermal conductivity (κ) was calculated using $\kappa = \alpha C_p \rho$. For measurements of density and specific heat capacity, three replicates were tested.

3. Results and discussion

Preparing GNs by reduction of graphite oxide (GO) is a scalable and versatile approach that is well-suited to chemical functionalization. GO has been synthesized with high yields by means of the modified Hummers method,[45] which completely exfoliated the GO in water into single layer nanosheets by simple sonication.[46–48] In the presence of SDBS, we handled the reduced SLGNs with aryl diazonium salts following a method similar to that of Tour *et al.*[49] so that the ATRP initiator was covalently linked to the nanosheet surface. Subsequent polymerization allowed PS chains to grow from the SLGN surface. Methyl 2-bromopropionate (MBP) was used as a free initiator to control the chain propagation on the surface. The corresponding preparation process is illustrated in Scheme 1, which also illustrates how the grafting density and length of polymer chains were controlled by tuning the amount of the grafting initiator and the molar ratio of components. Table 1 shows the reaction conditions used and summarizes the experimental results. With increasing monomer concentrations, the number average molecular weight (M_n) of grafting PS chains increases from 21 300 to 78 900 along with polydispersities of 1.6, 1.9 and 1.65 (in Table 1, refer to samples PS1-, PS2- and PS3-2-GNs). For the M_n determination of grafting PS, we first compared the molecular weights of the grafting PS cleaved from GNs (PS3-2-GNs) by an acid-catalyzed transesterification in 1-butanol with the GPC data obtained from the free, non-grafted PS. The corresponding GPC data are provided in Fig. S1 in ESI (Electronic Supplementary Information).† Except for the broadened molecular weight distribution, (polydispersity index: 1.73 and 1.65 for cleaved PS and free PS, respectively), the M_n of

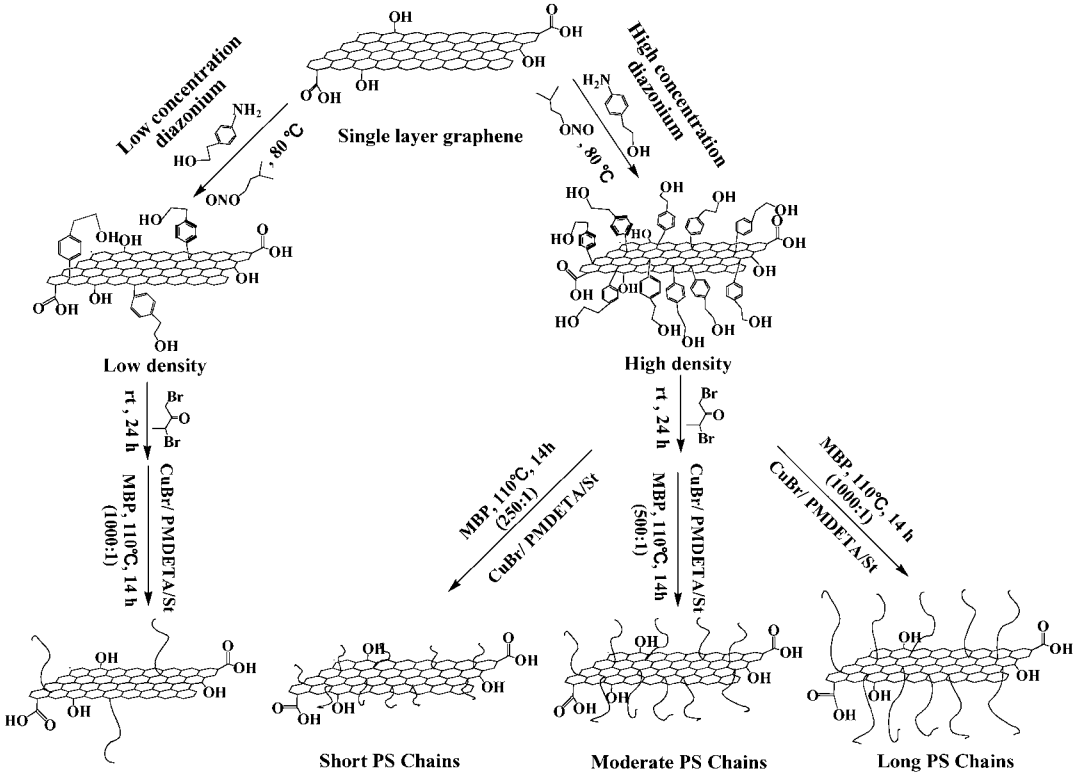

Scheme 1 Synthetic routes for achieving controllable functionalization of SLGNs.

the cleaved PS (76.8 kg mol^{-1}) is quite close to that of the free PS (78.8 kg mol^{-1}). This also agrees with the experimental observation of polymer brushes.[50] As a result, in this work, the M_ns of all grafting samples were determined by measuring the corresponding free PS inTHF.

To vary the grafting density, the concentration of diazonium salt during grafting of the initiator was varied, thereby controlling the amount of the bonded initiator (and thus the density of the grafting polymer). GPC results showed that M_n and polydispersity of the low grafting density sample (denoted as PS-1-GNs in Table 1) were 81 600 and 1.56, respectively, indicating a molecular size similar to that of PS3-2-GNs. However, the weight loss of PS-1-GNs at 600 °C was lower (55.4 wt%, compared with 85.5 wt% for PS3-2-GNs), indicating a difference in grafting density. In contrast, the range of weight losses of the PS-2-GN series (from 49.6 to 85.5 wt%) indicated a difference in grafted PS chain length (in view of the identical diazonium salt concentrations). Further discussion will be presented in combination with TEM characterization.

3.1. Evidence of single-layer graphene and covalent bonding

Exfoliation of GO nanosheets is a prerequisite for production of SLGNs, which depends on the type of pristine graphite, the oxidation conditions, and control of the interlayer cohesive energy.[51] The oxidation procedure practised here was sufficient to achieve complete exfoliation of GO nanosheets under sonication.[51] Fig. 1(a) shows a representative AFM image of GO nanosheets obtained by spin-coating a drop of 0.1 mg mL^{-1} GO aqueous solution onto a mica surface. The GO nanosheets obtained ranged from 0.5 to 1.5 μm. The mean lateral dimension was ~0.8 nm, and the average thickness was ~1 nm. The majority of the GO nanosheets were single-layered. Fig. 1(b) shows an AFM image of initiator-grafted GNs (Init-GNs) deposited on mica from a dilute DMF suspension. The thickness of Init-GNs increased to ~3 nm (from ~1 nm for the GO sheets). A similar increase was observed in chemically reduced GNs decorated with aryl groups such as nitrophenyl and chlorophenyl.[39,40] The height measured for those aryl-functionalized GNs was ~2.2 nm, and investigators concluded that the substituted aryl groups contributed ~0.6 nm in thickness (they assumed the bare GNs were 1 nm thick). Similarly, the 2 nm increase in thickness can be attributed to the initiator bonded to both sides of GNs, given the larger size of the initiator molecule compared with nitrophenyl or chlorophenyl groups. The observations indicate that the initiator molecules were linked to well-exfoliated, single-layer GNs.

The thickness of functionalized GNs should increase with increasing size of grafting groups or polymer molecules. Fig. 1(c) presents a representative AFM image of PS-grafted GNs (PS1-2-GNs). The PS1-2-GNs exhibited a rough surface and the average thickness increased by ~8 nm. Assuming a thickness of 1 nm for bare GNs, the thickness of the PS layers grafted on both sides was ~3.5 nm. Recall that the M_n of the grafting PS was 21 300, an approximate average square radius of gyration R_g can be estimated as $R_g \approx 0.028 \times \sqrt{M} = 4.05$ nm. This value is consistent with the AFM results and indicates a single-layered structure. The morphology of grafting PS differed from the homogeneous distribution of initiator on SLGNs. Some aggregated PS domains were discernable on the PS1-2-GNs and some

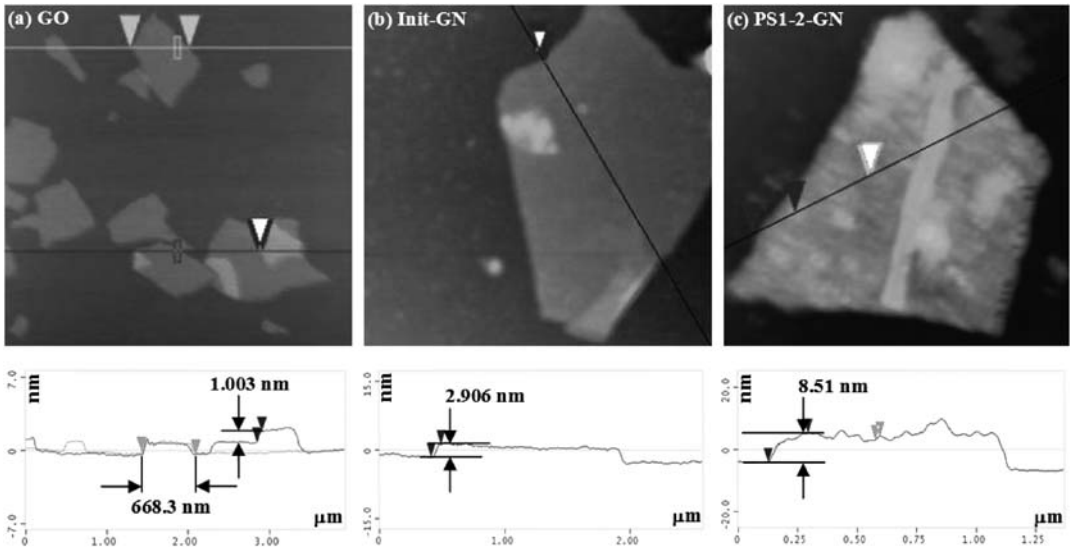

Fig. 1 AFM images of GO nanosheets, initiator- and PS-grafted GNs. All samples for AFM observations were prepared by spin-coating ~0.1 mg mL^{-1} dilute aqueous or DMF suspensions on mica surfaces. (a) GO nanosheets reveal the uniform distribution in the sheet thickness (~1 nm) except occasionally stacked fragments (two layers, as marked by three black arrows). (b) High density initiator-grafted GNs (Init-GNs) exhibit a relatively smooth surface (except for stacked fragments marked by a black arrow) and an average thickness of 2.9 nm. (c) High density low molecular weight PS-grafted GNs suggest a PS layer of 3.5 nm thick and an obvious pleat (marked by a black arrow) would be formed during spin-coating, reflecting the dependence of a rough grafting surface on the process of sample preparation.

preferred orientation was evident, possibly a consequence of the force imposed during spin-coating. Non-homogeneous PS aggregates on PS-GNs appears to be inconsistent with AFM observations of the Init-GNs (Fig. 1b). This issue will be addressed when TEM observations are presented.

X-Ray diffraction (XRD) patterns provided insight into the exfoliated structure of PS-GNs. In Fig. 2, XRD patterns from GO, PS-GNs, and pristine graphite are presented. The characteristic 0.34 nm basal plane spacing for the pristine graphite completely disappeared in the GO pattern, and a broad peak arose at 10.19°. The latter peak corresponds to an interlayer spacing of 0.87 nm and was attributed to the presence of oxygen-containing groups. In contrast, the PS-GNs pattern showed no peak, implying extensive exfoliation of PS-GNs. Note that the XRD measurements for the GO sample were conducted using dried powder without sonication, while the PS-GN sample was prepared by precipitating the suspension containing PS-GNs with methanol. In addition, complete disappearance of the characteristic diffraction peak for PS-GNs indicates that the stacked fragments observed in AFM (Fig. 1(a)) were relatively rare.

Both oxidation and covalent functionalization generally introduce defects in graphite and graphene sheets.[1,2] The defects are often manifest in spectroscopic data, from which additional structural information can be derived. Representative Raman spectra for the pristine graphite, GO and PS-1-GN samples are

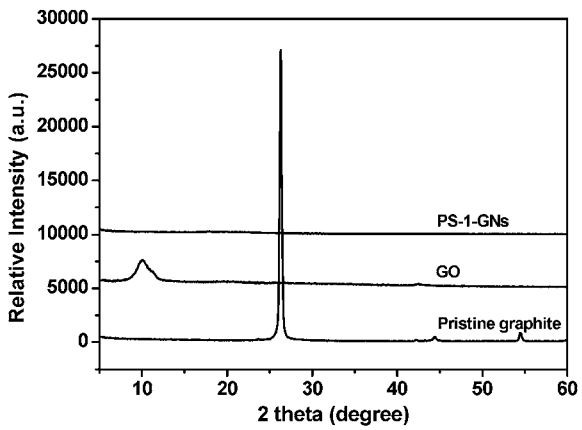

Fig. 2 XRD patterns of pristine graphite, GO nanosheets and PS-1-GN powder samples (Cu-Kα radiation $\lambda = 1.54$ Å at 0.02° s^{-1}). Complete disappearance of two peaks at 26.3 and 10.2° for PS-1-GNs indicates a well-exfoliated, single-layer structure.

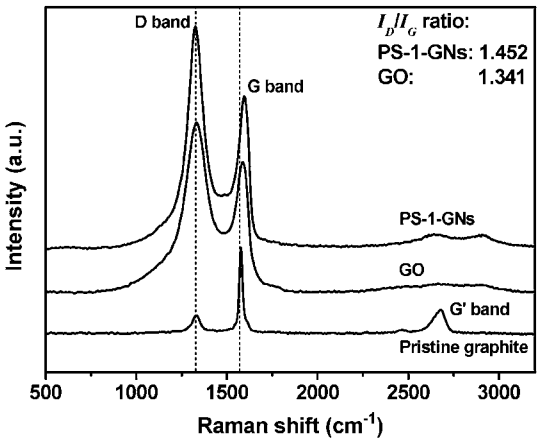

Fig. 3 Raman spectra of pristine graphite, GO nanosheets and PS-1-GNs (excitation wavelength 631 nm). The remarkably increased absorption intensity ratio at D and G bands reflects the covalent bonding between GNs and PS chains.

shown in Fig. 3. For the pristine graphite powder, three characteristic peaks were generated at 1325 (D band), 1578 (G band) and 2678 cm^{-1} (G′ band). The G band arises primarily from the presence of a sp^2 carbon network, while the D band originates from defects inherent in the graphite and the edge effect of graphite crystallites.[52] Generally, a perfect graphite crystal does not exhibit the D band. However, for most commercial graphite products, high-temperature treatments adopted during production inevitably introduce defects and reduce crystallite sizes, increasing edge effects.[53,54] The G′ band, also called the 2D band and an overtone of the D band, is sensitive to stacking order in the pristine graphite.[52] The barely visible G′ band for both the GO and PS-GNs indicates a near-absence of stacking order and/or the presence of exfoliated states. For GNs, a simple method to calculate crystallite size L_a has been proposed,[52,55] *i.e*, $L_a(\text{nm}) = (2.4 \times 10^{-10}) \times \lambda_{\text{laser}}^4 (I_D/I_G)$ (λ_{laser} is the laser excitation wavelength, and I_D and I_G are the peak intensities of D and G bands). The method allows one to indirectly assess the density of graphene defects in terms of crystallite size. Based on the data in Fig. 3, three crystal sizes were obtained (186.5, 28.4 and 26.2 nm), corresponding to pristine graphite, GO and PS-1-GNs. The defect density introduced by oxidation was significant (reduced crystallite size). However, the crystallite size reduction resulting from covalent functionalization appeared to be more limited (from 28.4 to 26.2 nm). Note that the covalent functionalization was completed after reduction with hydrazine hydrate, and the aromaticity of reduced GNs should be partially restored in PS-GNs, implying crystallite sizes larger than 28.4 nm[37] and further supporting the assertion that covalent bonding resulted between PS and the GNs.

3.2. Control of grafting density and chain length

Methods to effectively tailor the interface structure of nanoparticles have been widely reported.[23–31] Living polymerizations such as ATRP afford a convenient tool to control the chain length of the grafting polymer, while grafting density may be altered by introducing non-reactive groups upon grafting the initiator molecules to the particle surface.[56] Diazonium addition has been used effectively for the surface decoration of carbon nanotubes (CNTs), allowing a wide range of reactive groups to be covalently linked to CNT side walls.[49] This process has allowed workers to graft polymers with different chain lengths to the CNT surface, including block and branched polymers. However, an efficient method to tune the grafting density of polymer chains by diazonium addition has not been well established to our knowledge. For GNs, achieving effective control of grafting density over a wide range remains a formidable challenge.

The combination of diazonium addition and ATRP affords a solution for this issue. The diazonium-to-CNT coupling follows a radical mechanism, in which the aryl groups are linked to CNTs and then release aryl radicals *via* a single electron transfer process.[57] By this process, in principle, one can control the amount of the ATRP initiator grafted to GNs by changing the concentration of the diazonium. Indeed, Nair and Strano *et al.* have demonstrated the feasibility of this approach by means of photoabsorption spectra, in which the number of 4-hydroxybenzenes bonded to the SWNT surface was changed by increasing the concentration of diazonium salt.[62] In our experiments, a similar method was employed to control the concentration of ATRP initiator on the GN surface, and thus the grafting density of the polymer chains.

In Fig. 4(a), we show thermogravimetric curves for GO and GN samples grafted with phenyl ethanol and ATRP initiator. All examples were exhaustively washed and dried beforehand. GO is not thermally stable, and the mass loss started below 100 °C and became more rapid at 150 °C.[37] Organically modified GNs exhibited higher starting decomposition temperatures, which arose primarily from partial restoration of the aromatic structure in GO sheets. Notice the thermal behavior of samples in the temperature range 150–300 °C (see the rectangle marked in Fig. 4(a)). For GO sheets, most of the functional groups containing oxygen were lost in this temperature range, while for GNs with organic molecules, the weight loss was reduced. The extent of reduction in weight loss varied with the grafting density and the size of organic molecules. For the high density sample (Init-GN-2), the weight loss below 250 °C was slow, while at higher temperatures, the rate of weight loss accelerated quickly. Bromine scavenges free radicals during thermal decomposition[58] and thus the slower weight loss for Init-GN-2 was attributed to the effect of bromine. Once bromine is exhausted, however, decomposition of organic molecules ensues rapidly. For the low density sample (Init-GN-1), the stabilizing effect of bromine was less pronounced because of fewer grafting initiator molecules. Nevertheless, the stabilizing effect was greater (up to 250 °C) when compared with the decomposition behavior of GN-1-OH. Clearly, the data shown in Fig. 4(a) reflect the difference in the number and size of grafting molecules on GNs. For example, the grafting densities of phenethyl alcohol groups on GNs can be estimated to be ~1 functional groups in 49 carbon atoms for the high grafting density sample and in 73 carbon atoms for the low density sample. This is consistent with the results reported by Tour *et al.*,[39] where they observed that the grafting density of some aromatic groups such as chlorophenyl and nitrophenyl groups on GNs was ~1 functional group in 55 carbon atoms.

Chain length modulation of grafting polymers was achieved by controlling the molar ratio of monomer and initiator during polymerization. Three different lengths of PS chains (M_n = 21 300, 35 600 and 78 900, respectively) were linked to the GN surface by the ATRP initiator pre-bonded to GNs. When the grafting density of the polymer remained constant, the thickness of the grafting layer changed, which was observed directly in the weight loss behavior. Fig. 4(b) shows TGA curves for the three PS-GNs under the same conditions. For comparison, the TGA curves of pure PS (M_n = 78 900) and two GN samples containing different densities of ATRP initiator are also included. As before, the prominent weight loss of the GNs decorated with small molecules occurred primarily below 300 °C. However, for PS-grafted GNs, the rapid weight loss took place primarily between 350 and 450 °C, indicating markedly increased thermal stability. Among the samples shown in Fig. 4(b), pure PS exhibited the greatest thermal stability, showing negligible weight loss below 350 °C, and a delay in rapid decomposition to ~400 °C. For the three PS-GN samples, the thermal stability was gradually improved with increasing molecular weight of grafting PS (note the rectangular area marked). Likewise, the onset of weight loss at ~150 °C arose from decomposition of residual

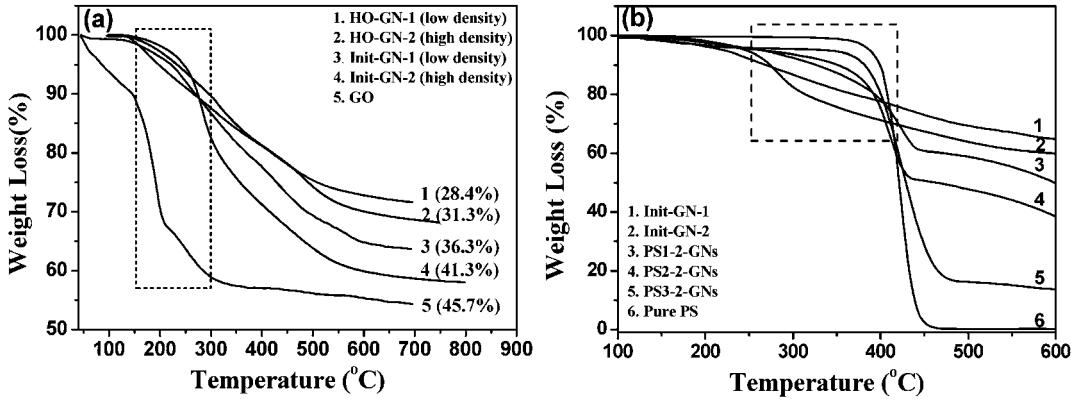

Fig. 4 (a) TGA curves of GO nanosheets and GNs with different grafting densities of organic molecules. The percentages marked are the weight losses at 600 °C of corresponding samples, revealing the effect of molecular size and grafting density. The weight loss behavior in the rectangular area suggests the scavenging effect of bromine for free radicals produced during the decomposition, reflecting the difference in grafting density of initiators. (b) TGA curves of pure PS and initiator- and PS-grafted GNs. The weight loss behavior in the rectangular area shows the inhibition effect of grafted PS on the decomposition of oxygen-containing groups on SLGNs, reflecting the difference in chain length of grafted PS.

oxygen-containing groups on the GNs.[37] Increasing thermal stability with increasing molecular size indicates that the grafted PS layer inhibited decomposition of residual groups on GNs, due to larger coverage ratios and thicker polymer layers. This assertion is supported by the increased weight loss of the three PS-GN samples at ~600 °C (Table 1). The assertion is also consistent (qualitatively) with the size of the grafting PS molecules, in view of the nearly identical residual functional groups and grafting densities of the three samples.

Fig. 5(a) and (b) present the morphological differences between low- and high-grafting density PS-GNs. The low-density sample (PS-1-GN, Fig. 5(a)) exhibits lateral dimensions of 0.6–1.5 mm, in accord with AFM observations (Fig. 1). Two PS-GNs in Fig. 5(a) appear to overlap, a consequence of the sample deposition process. Dark elliptical spots on the GN surface are ubiquitous and reveal the morphology of the grafted PS chains. This morphology is distinct from the case of polymer-functionalized carbon nanotubes, where a relatively uniform polymer interface

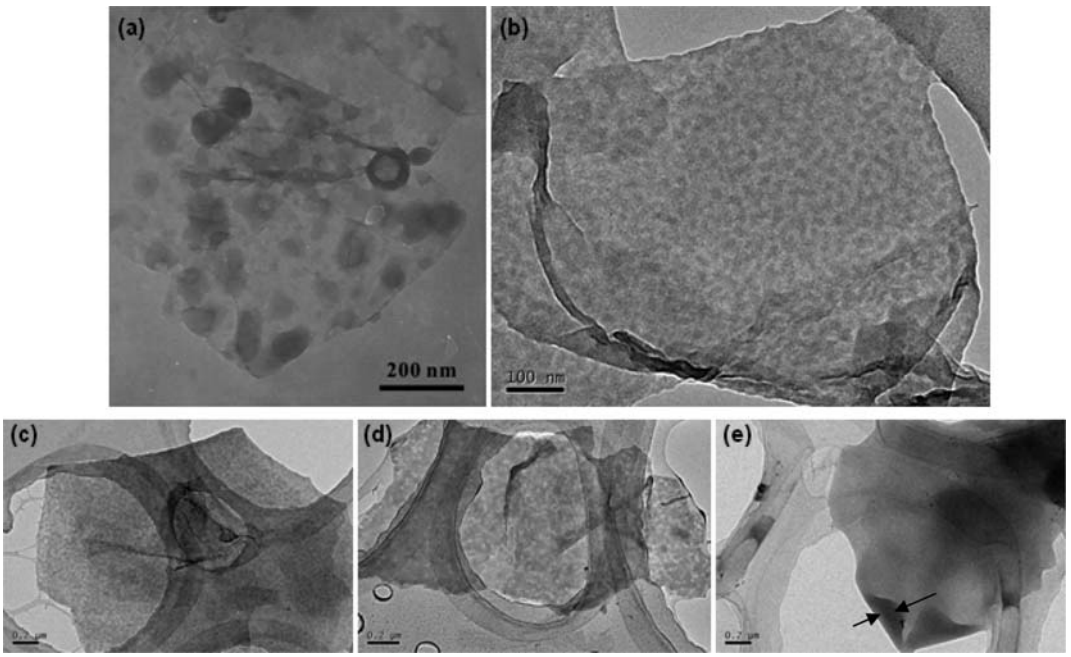

Fig. 5 TEM images of GNs with different grafting density and molecular weights of PS. (a) PS-1-GNs; (b) PS1-2-GNs; (c) PS1-2-GNs; (d) PS2-2-GNs; (e) PS3-2-GNs. All samples were prepared by depositing PS-GNs in dilute DMF suspensions on copper or holey carbon grids. (a) PS-1-GNs, PS grey granules (aggregates) distributed on GNs are not uniform, arising from the difference of local aromaticity. (b) PS1-2-GNs, uniform distribution of PS granules on GNs arises from high concentration of the diazonium compound in the system, which makes the effect of the local aromaticity difference negligible. (c) PS1-2-GNs, uniformly distributed granules are a characteristic morphology of high density low molecular weight PS-grafted sample. (d) PS2-2-GNs, increased molecular weights result in the formation of larger PS granules on GNs. (e) PS3-2-GNs, further increased molecular weights cause agglutination of contiguous PS aggregates on GNs so that the folded morphology appears after solvent evaporation, marked by black arrows.

layer is created.[59] The peculiar "condensed" (elliptical) morphology on the GN surface is related to the compatibility of PS and DMF. The solubility parameters of PS and DMF are 16.6–20.2 and 24.8 respectively, and thus DMF is a relatively poor solvent for PS.[60] Because of the solubility difference, PS chains cannot fully extend in DMF, leading to the formation of the observed condensed structure after drying. Similar phenomena have been reported for polymer brushes grafted onto substrates.[61]

The distribution of PS chains on the GN surface for PS-1-GNs was distinctly less uniform than for the high density PS1-2-GNs in which the PS forms a near-continuous coating. This is partially attributed to the aforementioned shielding effect of the surfactant (SDBS). In addition, the concentration of diazonium presumably affected the distribution of grafting chains. Note that in efforts to functionalize SWNTs, it has been observed that metallic SWNTs reacted more easily with diazonium salt than semiconducting SWNTs, particularly for low concentrations of diazonium compounds.[62] Thus, we conjecture that the observed variations in PS aggregate sizes resulted from differences in the local structure of individual GNs. Such structural variations in GNs reflect local aromaticity differences. For example, during preparation of PS-1-GNs, some radicals react preferentially with double bonds at metallic sites on GN surfaces. With increasing diazonium concentrations, however, such preference becomes negligible, and the majority of double bonds in GNs can undergo reaction, regardless of electronic structure.[62] For the present GNs, hydrazine reduction partially restored the aromaticity of GNs, although some surface defects were undoubtedly present. In this case, decreased aromaticity changed the reactivity of GNs and affected the distribution of grafting PS chains. This implies that the distribution uniformity of polymer chains (or surface roughness) on GNs can be tuned to some extent, simply by varying the amount of diazonium used (if grafting density control is not required).

Fig. 5(c)–(e) show the TEM images of three PS-GNs with different molecular weights but identical grafting densities. For the low molecular weight PS-grafted GN (PS1-2-GNs), the distribution of PS (gray granules) on the GN surface appeared uniform. Unlike PS-1-GNs (low grafting density), the size distribution of the gray granules also appears uniform. As the molecular weight increased, the size of granular domains (PS aggregates) also increased and became more irregular, suggesting the occurrence of agglutination between separately grafted PS chains.[63] Such agglutination between grafting chains became increasingly apparent so that the granular contrast observed in both PS1-2-GNs and PS2-2-GNs became barely distinguishable in the high molecular weight sample (PS3-2-GNs), where discrete granules were absent. Increased molecular weights increased the tendency for aggregation of polymer chains during solvent evaporation, thus leading to the folded morphology of PS-GNs (marked by the black arrows in Fig. 5(e)) due to agglutination. Combined with the TGA results, the TEM images illustrated distinct differences in the thermal behavior and morphology of different PS-GNs, and demonstrated the potential for tuning the interface structure.

3.3. Confined relaxation and improved heat conduction

Glass transition temperature (T_g) characterizes the segmental motion of polymers, which is strongly dependent on the interface structure in polymer-grafted nanoparticles and nanocomposites.[64–66] The strength and nature of the interface interaction may cause T_g to increase, decrease or remain constant.[31] For covalently grafted polymer chains, increases in T_gs are commonly observed due to the confinement of substrates or particles. Fig. 6 shows DSC curves for low- and high-density PS-GN powder samples with the corresponding T_g values marked for each sample. For comparison, the DSC curves for free/pure PS powder samples produced simultaneously during the grafting polymerization are also included. For the pure PS samples, T_g values increased with increasing molecular weight (from 85.7 to 93.5 °C), which is in accord with the rule established by Flory *et al.*[67] The T_g values were slightly lower than the results reported elsewhere,[67] a discrepancy that may arise from the difference in sample densities (that is, looser chain packing in powder samples relative to bulk samples, and thus less confinement and lower thermal conductance). In contrast, the PS-GNs exhibited higher T_g values. The low-density sample (PS-1-GN) showed an 8.7 °C increase in T_g compared to the pure PS sample with similar molecular weight (pure PS3). This increase was less than that observed in the high-density samples (*e.g.*, PS3-2-GNs showed a 15.2 °C increase in T_g). For the high-density samples, the low M_n sample showed the largest increase in T_g (as much as 18 °C, from 85.7 to 103.7 °C), indicating a substantial confinement effect of GNs on the segmental motion of PS chains. Generally, segments in closer proximity to the substrate or particle surface experience stronger confinement relative to those segments farther away.[31] Shorter PS chains grafted on GNs (PS1-2-GNs) have more strongly confined segments compared to longer PS chains (PS3-2-GNs). It is thus not surprising that PS1-2-GNs exhibit a larger T_g increase (18 °C) than PS3-2-GNs (15.2 °C). In addition, with increasing molecular weight, the PS-GN samples showed a smaller increase in T_g (from 103.7 to 108.7 °C) than the corresponding pure PS samples (from 85.7 to 93.5 °C). Furthermore, changes in heat capacity (ΔC_p, which can be approximated by differences in heat flows near T_g[68]) during the glass transition are different for the pure PS and PS-GNs. For the pure PS samples, ΔC_p increased with increasing molecular weight because of decreased chain packing densities. This

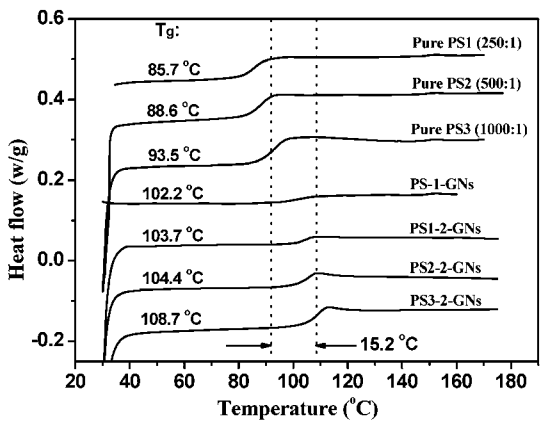

Fig. 6 DSC curves of pure PS and different PS-GN powder samples under the same condition: heating rate 10 °C min^{-1} and nitrogen as a purge gas. The thermal history of all samples was eliminated by heating to 180 °C at 20 °C min^{-1} and kept there for 5 min.

observation is similar to the case of PS-GNs, although PS-GNs exhibit a smaller heat flow step during the glass transition. The most pronounced variation in T_g was observed in the PS-1-GNs sample, in which the GNs content was the greatest relative to other PS-GNs. Because of the influence of heat conductance on DSC measurements, the incorporation of GNs significantly affects the thermal properties of the composites. To support this claim, the thermal conductivities of PS films with different GN contents were examined.

The measured thermal conductivity of mechanically exfoliated single layer graphene at room temperature is reportedly as high as ~5000 W m^{-1} K.[69] However, the thermal conductivity of GNs produced by reducing graphite oxide is largely unknown, so we evaluated the effect of GNs on the thermal conductivity of polymer composites. To achieve this, PS-grafted GNs were dispersed in toluene and then mixed with PS solutions with different solid contents, followed by a drop-casting procedure to prepare polymer/composite films. The weight percentages of GNs in PS nanocomposites do not include the weight of PS grafted on GNs, that is, the PS weight in PS-GNs has been deducted in terms of TGA results in determining the graphene contents in the PS nanocomposites. Because of good compatibility between PS-GNs and the matrix, the dispersion of GNs in PS is quite homogeneous. Fig. 7 presents the representative SEM fractographs of the neat PS and PS composite with 2 wt% PS1-2-GNs. The fracture surface of the neat PS sample is smooth, except for some residual fragments. In contrast, the fracture surface of the GN-PS composite appears to be slightly rough (for clarity, a larger magnification was used to observe the composite sample), in which some tiny protuberances can be distinguished. In fact, it has been a challenge to clearly observe the dispersion of GNs in polymer matrices due to its electronic transparency so that in some contexts one only observes the profile of GNs due to the scattering effect of the edge, as shown in Fig. 5. In this case, those tiny protuberances would reflect the dispersion of GNs in the PS matrix and homogeneously distributed protuberances suggest a good dispersion status.

Fig. 8 presents the results of PS films containing different GN contents, in which the corresponding error bars obtained from three measurements are also displayed. These films were prepared by dispersing different amounts of PS1-2-GNs or PS-1-GNs in a toluene solution containing PS and following a drop-casting procedure. The thermal conductivity of the pure PS film was 0.158 W m^{-1} K, which is similar to the reported value of

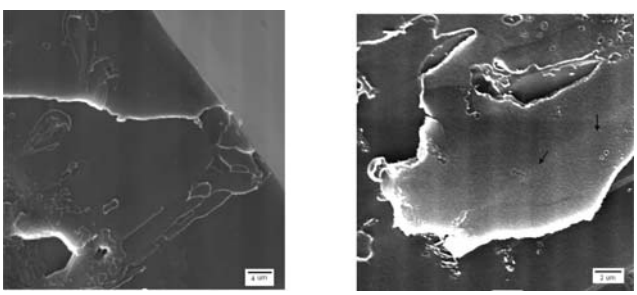

Fig. 7 SEM fractographs of the neat polystyrene and nanocomposites with 2 wt% PS1-2-GNs in polystyrene matrix. The stubs marked by black arrows are graphene nanosheets imbedded in the polystyrene matrix.

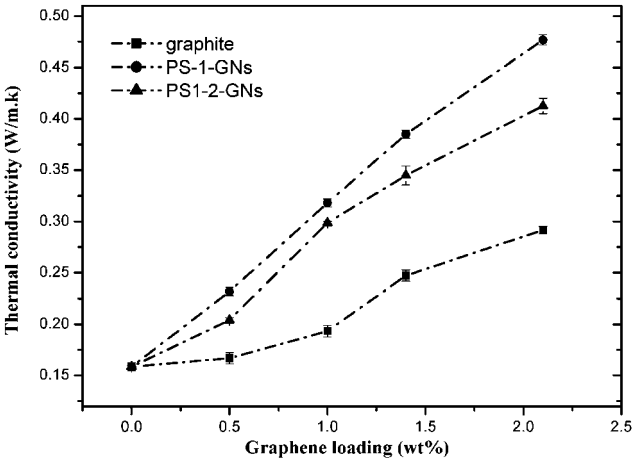

Fig. 8 The measured thermal conductivities at 35 °C of the pure PS and composite films with different contents of PS1-2-GNs, PS-1-GNs and raw graphite. The error bar for each sample was obtained from three measurements.

0.133 W m^{-1} K.[70] With increasing GN content, the thermal conductivities of the composite films increased in approximately linear fashion. The thermal conductivity at 35 °C of the composite film with a 2.0 wt% GN content was 0.413 W m^{-1} K, or 2.6 times that of the pure PS film (a 161% increase). This is superior to results reported for single-walled carbon nanotube (SWNT)-PS composites, where a room temperature value of ~0.36 W m^{-1} K was obtained for samples with 5 vol% loading.[69] Similar improvements observed in GN-epoxy systems were attributed to the smaller interface fraction in GN composites relative to SWNTs.[71,72] In polymer composites, phonon acoustic scattering at the interface also plays an important role in the heat conductance efficiency. A reduced interface fraction or effective interface link translates to reduced thermal resistance.[73] In this sense, control of interface structure is also beneficial for optimization of thermal properties of GN-based nanocomposites. To further observe the possible effect of GN-PS interface structure, the thermal conductivities of the low grafting density composites with PS-1-GNs and the unmodified graphite filled PS composites were also drawn as a function of solid contents in Fig. 8. Unmodified graphite filled PS composites revealed less improvement in thermal conductivity due to poor dispersion and interface interaction. However, the low grafting density composites exhibited higher thermal conductivities than those high grafting density samples. This reflects the importance of thermal conductivity of graphene itself. It is conjectured that covalent bonding diminishes the aromaticity of GNs and thus impairs their thermal conductance efficiency. In this sense, it is necessary to balance the GN-polymer interface structure and the intrinsic properties of GNs upon optimizing the performance of GN-based composites.

4. Conclusion

The exceptional properties of graphene afford an opportunity to develop high-performance polymer nanocomposites, although this opportunity depends largely on the ability to design and control interface structure. We have demonstrated the ability to

systematically tune the grafting density and chain length of polymer molecules covalently bonded to single-layer graphene nanosheets (SLGNs) by combining diazonium addition and atomic transfer radical polymerization (ATRP). Our results showed that in the high grafting density samples, the distribution of grafting polymer chains on SLGNs was more uniform compared to the low grafting density sample. The difference in grafting chain distributions was attributed to the preference of diazonium compounds for metallic sites in SLGNs, an assertion that arose from an earlier study of the reactivity of diazonium compounds with metallic and non-metallic carbon nanotubes. The relaxation of the polymer chains covalently bonded to the SLGN surface was strongly confined, particularly for segments in close proximity to the SLGN surface. The confinement effect was accompanied by enhanced thermal conductivity of GNs composites—substantial increases in thermal conductivity of SLGN-PS nanocomposites were observed for SLGN contents of only 2.0 wt%.

Acknowledgements

This work was supported by the National Basic Research Program of China (Grant No. 2005CB623800), NSF of China (Grant No.50573014 and No.50773012), Shanghai Basic Research Program (Grant No.05JC14002). H. L. and Y. Y. are also grateful for the support of NSFC program "Excellence in Research Group" (Grant No. 20221402).

Notes and references

1 (*a*) A. K. Geim and K. S. Novoselov, *Nat. Mater.*, 2007, **6**, 183–191; (*b*) A. K. Geim, *Science*, 2009, **324**, 1530–1534.
2 S. J. Park and R. S. Ruoff, *Nat. Nanotechnol.*, 2009, **4**, 217–224.
3 S. P. Pang, H. N. Tsao, X. L. Feng and K. Mullen, *Adv. Mater.*, 2009, **21**, 3488.
4 G. C. Liang, N. Neophytou, M. S. Lundstrom and D. E. Nikonov, *Nano Lett.*, 2008, **8**, 1819–1824.
5 Q. Su, S. P. Pang, V. Alijani, C. Li, X. L. Feng and K. Mullen, *Adv. Mater.*, 2009, **21**, 3191.
6 X. Wang, L. J. Zhi, N. Tsao, Z. Tomovic, J. L. Li and K. Mullen, *Angew. Chem., Int. Ed.*, 2008, **47**, 2990–2992.
7 J. Atalaya, A. Isacsson and J. M. Kinaret, *Nano Lett.*, 2008, **8**, 4196–4200.
8 Y. Y. Liang, D. Q. Wu, X. L. Feng and K. Mullen, *Adv. Mater.*, 2009, **21**, 1679–1683.
9 M. D. Stoller, S. Park, Y. W. Zhu, J. H. An and R. S. Ruoff, *Nano Lett.*, 2008, **8**, 3498–3502.
10 T. Ramanathan, A. A. Abdala, S. Stankonich, D. A. Dikin, M. Herrera-Alonso, R. D. Piner, D. H. Adamson, H. C. Schniepp, X. Chen, R. S. Ruoff, S. T. Nguyen, I. A. Aksay, R. K. Prud'homme and L. C. Brinson, *Nat. Nanotechnol.*, 2008, **3**, 327–331.
11 S. Stankovich, D. A. Dikin, G. H. B. Dommett, K. M. Kohlhaas, E. J. Zimney, E. A. Stach, R. D. Piner, S. T. Nguyen and R. S. Ruoff, *Nature*, 2006, **442**, 282–286.
12 J. S. Wu, W. Pisula and K. Mullen, *Chem. Rev.*, 2007, **107**, 718–747.
13 J. Sakamoto, J. van Heijst, O. Lukin and A. D. Schluter, *Angew. Chem., Int. Ed.*, 2009, **48**, 1030–1069.
14 V. C. Tung, M. J. Allen, Y. Yang and R. B. Kaner, *Nat. Nanotechnol.*, 2009, **4**, 25–29.
15 M. Choucair, P. Thordarson and J. A. Stride, *Nat. Nanotechnol.*, 2009, **4**, 30–33.
16 X. L. Li, G. Y. Zhang, X. D. Bai, X. M. Sun, X. R. Wang, E. G. Wang and H. J. Dai, *Nat. Nanotechnol.*, 2008, **3**, 538–542.
17 Y. Hernandez, V. Nicolosi, M. Lotya, F. M. Blighe, Z. Y. Sun, S. De, I. T. Mcgovern, B. Holland, M. Byrne, Y. K. Gun'Ko, J. J. Boland, P. Niraj, G. Duesberg, S. Krishnamurthy, R. Goodhue, J. Hutchison, V. Scardaci, A. C. Ferrari and J. N. Coleman, *Nat. Nanotechnol.*, 2008, **3**, 563–568.
18 S. Niyog, E. Bekyarova, M. E. Itkis, J. L. McWilliams, M. A. Hamon and R. C. Haddon, *J. Am. Chem. Soc.*, 2006, **128**, 7720–7721.
19 Y. C. Si and E. T. Samulski, *Nano Lett.*, 2008, **8**, 1679–1682.
20 J. I. Paredes, S. Villar-Rodil, A. Martinez-Alonso and J. M. D. Tascon, *Langmuir*, 2008, **24**, 10560–10564.
21 L. J. Cote, F. Kim and J. X. Huang, *J. Am. Chem. Soc.*, 2009, **131**, 1043–1049.
22 M. Lotya, Y. Hernandez, P. J. King, R. J. Smith, V. Nicolosi, L. S. Karlsson, F. M. Blighe, S. De, Z. M. Wang, I. T. McGovern, G. S. Duesberg and J. N. Coleman, *J. Am. Chem. Soc.*, 2009, **131**, 3611–3620.
23 Y. J. Min, M. Akbulut, K. Kristiansen, Y. Golan and J. Israelachvili, *Nat. Mater.*, 2008, **7**, 527–538.
24 D. W. Boukhvalov and M. I. Katsnelson, *Nano Lett.*, 2008, **8**, 4373–4379.
25 D. Konatham and A. Striolo, *Nano Lett.*, 2008, **8**, 4630–4641.
26 A. Bansal, H. C. Yang, C. Z. Li, K. W. Cho, B. C. Benicewicz, S. K. Kumar and L. S. Schadler, *Nat. Mater.*, 2005, **4**, 693–698.
27 P. Rittigstein, R. D. Priestley, L. J. Broadbelt and J. M. Torkelson, *Nat. Mater.*, 2007, **6**, 278–282.
28 A. C. Balazs, T. Emrick and T. P. Russell, *Science*, 2006, **314**, 1107–1110.
29 S. C. Warren, F. J. Disalvo and U. Wiesner, *Nat. Mater.*, 2007, **6**, 156–161.
30 M. E. Mackay, A. Tuteja, P. M. Duxbury, C. J. Hawker, B. V. Horn, Z. B. Guan, G. H. Chen and R. S. Krishnan, *Science*, 2006, **311**, 1740–1743.
31 H. J. Oh and P. F. Green, *Nat. Mater.*, 2009, **8**, 139–143.
32 (*a*) Y. X. Xu, H. Bai, G. W. Lu, C. Li and G. Q. J. Shi, *J. Am. Chem. Soc.*, 2008, **130**, 5856–5857; (*b*) H. Bai, Y. X. Xu, L. Zhao, C. Li and G. Q. Shi, *Chem. Commun.*, 2009, 1667–1669.
33 Z. Liu, J. T. Robinson, X. M. Sun and H. J. Dai, *J. Am. Chem. Soc.*, 2008, **130**, 10876–10877.
34 S. Stankovich, R. D. Piner, X. Q. Chen, N. Q. Wu, S. T. Nguyen and R. S. Ruoff, *J. Mater. Chem.*, 2006, **16**, 155–158.
35 F. M. Koehler, N. A. Luechinger, D. Ziegler, E. K. Athanassiou, R. N. Grass, A. Rossi, C. Hierold, A. Stemmer and W. J. Stark, *Angew. Chem., Int. Ed.*, 2009, **48**, 224–227.
36 J. F. Shen, Y. H. Hu, C. Li, C. Qin and M. X. Ye, *Small*, 2009, **5**, 82–85.
37 S. Stankovich, R. D. Piner, S. T. Nguyen and R. S. Ruoff, *Carbon*, 2006, **44**, 3342–3347.
38 G. Eda and M. Chhowalla, *Nano Lett.*, 2009, **9**, 814–818.
39 J. R. Lomeda, C. D. Doyle, D. V. Kosynkin, W. F. Hwang and J. M. Tour, *J. Am. Chem. Soc.*, 2008, **130**, 16201–16206.
40 E. Bekyarova, M. E. Itkis, P. Ramesh, C. Berger, M. Sprinkle, W. A. de Heer and R. C. Haddon, *J. Am. Chem. Soc.*, 2009, **131**, 1336–1337.
41 S. Niyogi, E. Bekyarova, M. E. Itkis, J. L. McWilliams, M. A. Hamon and R. C. Haddon, *J. Am. Chem. Soc.*, 2006, **128**, 7720–7721.
42 L. M. Veca, F. S. Lu, M. J. Meziani, L. Cao, P. Y. Zhang, G. Qi, L. W. Qu, M. Shrestha and Y. P. Sun, *Chem. Commun.*, 2009, 2565–2567.
43 M. Fang, H. B. Lu, Y. L. Yang and S. Nutt, *J. Mater. Chem.*, 2009, **19**, 7098.
44 X. S. Li, W. W. Cai, J. H. An, S. Kim, J. Nah, D. X. Yang, R. Piner, A. Velamakanni, I. Jung, E. Tutuc, S. K. Banerjee, L. Colombo and R. S. Ruoff, *Science*, 2009, **324**, 1312–1314.
45 (*a*) W. S. Hummers and R. E. J. Offeman, *J. Am. Chem. Soc.*, 1958, **80**, 1339; (*b*) S. Gilje, S. Han, M. Wang, K. L. Wang and R. B. Kaner, *Nano Lett.*, 2007, **7**, 3394.
46 Y. C. Si and E. T. Samulski, *Nano Lett.*, 2008, **8**, 1679–1682.
47 J. I. Paredes, S. Villar-Rodil, A. Martinez-Alonso and J. M. D. Tascon, *Langmuir*, 2008, **24**, 10560–10564.
48 S. J. Park, J. H. An, I. H. Jung, R. D. Piner, S. J. An, X. S. Li, A. Velamakanni and R. S. Ruoff, *Nano Lett.*, 2009, **9**, 1593–1597.
49 C. A. Dyke and J. M. Tour, *J. Am. Chem. Soc.*, 2003, **125**, 1156–1157.
50 (*a*) M. Husseman, E. E. Malmstrom, M. McNamara, M. Mate, D. Mecerreyes, D. G. Benoit, J. L. Hedrick, P. Mansky, E. Huang, T. P. Russell and C. J. Hawker, *Macromolecules*, 1999, **32**, 1424–1431; (*b*) J. Pyun, S. J. Jia, T. Kowalewski, G. D. Patterson and K. Matyjaszewski, *Macromolecules*, 2003, **36**, 5094–5104.
51 Z. S. Wu, W. C. Ren, L. B. Gao, B. L. Liu, C. B. Jiang and H. M. Cheng, *Carbon*, 2009, **47**, 493–499.

52 M. A. Pimenta, G. Dresselhaus, M. S. Dresselhaus, L. G. Cancado, A. Jorio and R. Saito, *Phys. Chem. Chem. Phys.*, 2007, **9**, 1276–1291.
53 K. N. Kudin, B. Ozbas, H. C. Schniep, R. K. Prud'homme, I. A. Aksay and R. Car, *Nano Lett.*, 2008, **8**, 36–41.
54 S. Reich and C. Thomsen, *Philos. Trans. R. Soc. London, Ser. A*, 2004, **362**, 2271–2288.
55 L. Cancado, K. Takai, T. Enoki, M. Endo, Y. A. Kim, H. Mizusaki, A. Jorio, L. N. Coelho, R. Magalhaes-Paniago and M. A. Pimenta, *Appl. Phys. Lett.*, 2006, **88**, 163106.
56 N. V. Tsarevsky and K. Matyjaszewski, *Chem. Rev.*, 2007, **107**, 2270–2299.
57 G. Schmidt, S. Gallon, S. Esnouf, J. P. Bourgoin and P. Chenevier, *Chem.–Eur. J.*, 2009, **15**, 2101–2109.
58 F. Laoutid, L. Bonnaud, M. Alexandre, J. M. Lopez-Cuesta and P. Dubois, *Mater. Sci. Eng., R*, 2009, **63**, 100–125.
59 L. Xie, F. Xu, F. Qiu, H. B. Lu and Y. L. Yang, *Macromolecules*, 2007, **40**, 3296–3305.
60 Y. S. Yu and A. Eisenberg, *J. Am. Chem. Soc.*, 1997, **119**, 8383–8384.
61 B. Zhao, R. T. Haasch and S. MacLaren, *J. Am. Chem. Soc.*, 2004, **126**, 6124–6134.
62 N. Nair, W. J. Kim, M. L. Usrey and M. S. Strano, *J. Am. Chem. Soc.*, 2007, **129**, 3946–3954.
63 (*a*) D. Li and R. B. Kaner, *J. Am. Chem. Soc.*, 2006, **128**, 968–975; (*b*) P. J. Costanzo, N. Dan, K. S. Lancaster, C. B. Lebrilla and T. E. Patten, *Macromolecules*, 2008, **41**, 1570–1576.
64 P. G. Debenedetti and F. H. Stillinger, *Nature*, 2001, **410**, 259–267.
65 C. J. Ellison and J. M. Torkelson, *Nat. Mater.*, 2003, **2**, 695–670.
66 H. B. Lu and S. Nutt, *Macromolecules*, 2003, **36**, 4010–4016.
67 T. G. Fox Jr. and P. J. Flory, *J. Appl. Phys.*, 1950, **21**, 581–591.
68 M. E. Brown. *Handbook of Thermal Analysis and Calorimetry*, Elsevier, Amsterdam, 1998; vol. 1.
69 C. Lee, X. Wei, J. W. Kysar and J. Hone, *Science*, 2008, **321**, 385.
70 J. E. Peters, D. V. Papavassiliou and B. P. Grady, *Macromolecules*, 2008, **41**, 7274–7277.
71 A. P. Yu, P. Ramesh, M. E. Itkis, E. Bekyarova and R. C. Haddon, *J. Phys. Chem. C*, 2007, **111**, 7565–7569.
72 L. M. Veca, M. J. Meziani, W. Wang, X. Wang, F. S. Lu, P. Y. Zhang, Y. Lin, R. Fee, J. W. Connell and Y. P. Sun, *Adv. Mater.*, 2009, **21**, 2088–2092.
73 K. I. Winey, T. Kashiwagi and M. Mu, *MRS Bull.*, 2007, **32**, 348–353.

